Branching in the Gaseous Reaction H + DCl as a Function of Collision Energy

V. J. Barclay, B. A. Collings, J. C. Polanyi,* and J. H. Wang†

Department of Chemistry, University of Toronto, Toronto, Ontario, Canada M5S 1A1
(Received: December 18, 1990)

Branching in the gas-phase reaction H + DCl → HD + Cl (I) (termed abstraction) and → HCl + D (II) (exchange) has been measured by monitoring the atomic products Cl and D by resonantly enhanced multiphoton ionization. The collision energy has been varied in the range 1.0–2.4 eV by alteration in the photolytic source of H. Within the error limits, the cross section for abstraction was found to remain constant at 0.16 ± 0.06 Å^2. The cross section for exchange exhibited a moderate decrease from 0.6 ± 0.3 to 0.2 ± 0.1 Å^2 with increasing collision energy. These findings concerning the abstraction reaction agree with the results of a quasi-classical trajectory computation, reported here, on the GQQ potential energy surface, the most reliable PES available [Schwenke, D. W.; et al. *J. Chem. Phys.* **1989**, *90*, 3110]. The experimental findings for exchange, however, stand in marked contrast to the trajectory results, suggesting that the exchange channel of the GQQ PES may be deficient in the region of high collision energies where the reacting system, en route to exchange, accesses bent intermediate configurations for which ab initio data are lacking.

I. Introduction

The system XH_2, where X is a halogen atom, played a seminal role in the field of gaseous reaction dynamics. The application of lasers to the determination of product energy distributions in such reactions was made by Parker and Pimentel[1] in 1969, only four years after their demonstration of the first chemical laser exploiting this same family of reactions.[2] The present study follows in this tradition by examining the reaction H + DCl → HD + Cl (termed "abstraction") and its alternate route H + DCl → HCl + D ("exchange") as a function of collision energy, using laser ionization to measure the yield of atomic products Cl and D. The extent of branching in the gaseous reaction is of potential interest in view of the fact that the outcome is sensitive to the direction of approach of H to DCl, as we shall demonstrate. Possibilities exist for controlling this direction of approach in two novel ways: inducing photoreaction in gaseous clusters[3] or in physisorbed monolayers.[4]

The reactions of H + HCl and its isotopic variants have been the subject of numerous experimental and theoretical studies.[5,6] These studies have led to well-established Arrhenius parameters for the abstraction reaction over the temperature range 200–500 K.[7] Less is known about the exchange reaction. Experimental estimates have placed the barrier height for exchange from as low as 5 kcal/mol[8] to as high as 22 kcal/mol.[9] Ab initio calculations yield barrier heights ranging from 18 to 26 kcal/mol.[10-13]

Recent studies[14,15] of the reaction H + HCl at a collision energy of 1.6 eV have measured the cross section for the abstraction channel to be 2 ± 1 Å^2, whereas the exchange plus energy-transfer channels (H rebounding from HCl) gave a combined cross section of 13 ± 3 Å^2. It has been shown by Wight et al.[5] that the dominant process is energy transfer; however, the cross section for the exchange reaction alone is not quantitatively known.

By use of the isotopic analogue to this reaction, H + DCl, one can distinguish exchange reaction from energy transfer. In the present study the cross sections for the abstraction and exchange reactions

$$H + DCl \rightarrow HD + Cl, Cl^* \qquad (I, I^*)$$

$$\rightarrow HCl + D \qquad (II)$$

have been measured as a function of collision energy over the range 1.0–2.4 eV. Isotopic scrambling, which in the past has led to widely disparate results,[6] has been avoided by the use of two separate nozzles for the reagents. The technique of resonantly enhanced multiphoton ionization (REMPI) coupled with time-of-flight mass spectrometry was used to observe the atomic products. Observation of the atomic products by REMPI has enabled us to estimate the individual reaction cross sections for abstraction leading to the alternative products Cl and Cl* (reactions I and I*).

The cross sections for the abstraction and exchange channels have also been computed in the present study using the quasi-classical trajectory (QCT) method. The "global" (GQQ) potential energy surface (PES) of Schwenke et al.[12] was employed. This PES is a modification of an earlier London–Eyring–Polanyi–Sato (LEPS) potential[16] that modeled the "backward abstraction" reaction at thermal energies with fair accuracy[17]

$$Cl + H_2 \rightarrow HCl + H \qquad (-I)$$

although it produced a well in the exchange channel, which was thought to be nonphysical.[6]

A comparison of the experimental and QCT results will be presented, indicative of the accuracy of the GQQ surface in this energy regime. Regions of the PES that are most crucial at these energies have been determined by examining sample trajectories leading to reaction. Rigid-molecule plots make possible a convenient presentation of the geometries of closest approach, leading

† Present address: Cameco Corporation, Research and Development, 225-15 Innovation Blvd., Saskatoon, Saskatchewan, Canada, S7N 2X8.

(1) Parker, J. H.; Pimentel, G. C. *J. Chem. Phys.* **1969**, *51*, 91.
(2) Kasper, J. V. V.; Pimentel, G. C. *Phys. Rev. Lett.* **1965**, *14*, 352. Pimentel, G. C. *Sci. Am.* **1966**, *214*, 32.
(3) Buelow, S.; Radhakrishnan, G.; Catanzarite, J.; Wittig, C. *J. Chem. Phys.* **1985**, *83*, 444. Shin, S. K.; Chen, Y.; Nickolaisen, S.; Sharpe, S. W.; Beaudet, R. A.; Wittig, C. Photoinitiated Reactions in Weakly-Bonded Complexes. In *Advances in Photochemistry*; Vol. 16, Chapter 5; Volman, D., Hammond, G., Neckers, D., John Wiley and Sons: Toronto, in press.
(4) Bourdon, E. B. D.; Cowin, J. P.; Harrison, I.; Polanyi, J. C.; Segner, J.; Stanners, C. D.; Young, P. A. *J. Phys. Chem.* **1984**, *88*, 6100. Bourdon, E. B. D.; Das, P.; Harrison, I.; Polanyi, J. C.; Segner, J.; Stanners, C. D.; Williams, R. J.; Young, P. A. *Faraday Discuss. Chem. Soc.* **1986**, *82*, 343. Polanyi, J. C.; Rieley, H. Photochemistry in the Adsorbed State. In *Advances in Gas-Phase Photochemistry*; Vol. 3; Ashfold, M. N. R., Rettner, C. T., Eds.; Royal Society of Chemistry: London, U.K., in press.
(5) Miller, J. C.; Gordon, R. J. *J. Chem. Phys.* **1983**, *78*, 3713 and references therein.
(6) Weston, Jr., R. E. *J. Phys. Chem.* **1979**, *83*, 61.
(7) Miller, J. C.; Gordon, R. J. *J. Chem. Phys.* **1981**, *75*, 5305.
(8) Endo, H.; Glass, G. P. *Chem. Phys. Lett.* **1976**, *44*, 180.
(9) Wight, C. A.; Magnotta, F.; Leone, S. R. *J. Chem. Phys.* **1984**, *81*, 3951.
(10) Botschwina, P.; Meyer, W. *Chem. Phys.* **1977**, *20*, 43.
(11) Dunning, Jr., T. H. *J. Chem. Phys.* **1977**, *66*, 2752.
(12) Schwenke, D. W.; Tucker, S. C.; Steckler, R.; Brown, F. B.; Lynch, G. C.; Truhlar, D. G. *J. Chem. Phys.* **1989**, *90*, 3110.
(13) Voter, A. F.; Goddard III, W. A. *J. Chem. Phys.* **1981**, *75*, 3638.
(14) Aker, P. M.; Germann, G. J.; Valentini, J. J. *J. Chem. Phys.* **1989**, *90*, 4795.
(15) Aker, P. M.; Germann, G. J.; Tabor, K. D.; Valentini, J. J. *J. Chem. Phys.* **1989**, *90*, 4809.
(16) Stern, M. J.; Persky, A.; Klein, F. S. *J. Chem. Phys.* **1973**, *58*, 5697.
(17) Tucker, S. C.; Truhlar, D. G.; Garrett, B. C.; Isaacson, A. D. *J. Chem. Phys.* **1985**, *82*, 4102.

0022-3654/91/2095-2921$02.50/0

to abstraction and exchange for various DCl internuclear separations.

II. Experimental Section

The experiments were carried out in a high-vacuum apparatus that has already been described in outline.[18] The apparatus embodied three stages of differential pumping. The first stage contained the interaction region where the counterpropagating photolysis (L_1) and probe (L_2) lasers intersected at right angles to the time-of-flight axis at a distance of approximately 3 mm below the free jet expansion. Two 120-μm-i.d. stainless steel nozzles were used for the expansion of the reagent gases. The nozzles were parallel and positioned 0.5 mm apart. Use of separate nozzles prevented the isotopic H/D scrambling between the "precursor" reagents H_2S, HBr, and HI employed in the photolytic formation of H and the second reagent DCl.

A backing pressure of 200 Torr was used for each reagent. This produced a partial pressure of 20 mTorr in the interaction region from each gas, ensuring single-collision conditions at the detection times used. The interaction region was located within the first acceleration stage of a two-stage Wiley-McLaren type mass spectrometer[19] in which an electric field strength of 1250 V/cm was used. Biasing the nozzles to ~3800 V reduced their effect upon the electric field lines in this region.

The second vacuum chamber contained the next acceleration stage of the mass spectrometer and a Wien filter (Colutron Corp., Model 300). The Wien filter dispersed the ions along a plane perpendicular to the time-of-flight axis. This allowed the use of high detector gains without saturation effects due to unwanted signals.

The third vacuum chamber contained a Chevron dual multichannel plate detector (MCP) which provided signal gains of up to 10^8. This stage contained a time-of-flight drift region with a length of 65 cm and mass resolution of $m/\Delta m = 200$. The resulting signal was preamplified by two 300-MHz amplifiers (Philips Scientific, Model 6950), with a gain of 10 each, and then processed by a boxcar integrator (Stanford Research, SR250) using a 100-ns sampling gate. The signal was collected, on a shot-to-shot basis, by an analog input/output device (Stanford Research, SR245), which acted as an interface to a Macintosh SE computer. Laser powers were also monitored and collected on a shot-to-shot basis.

Triggering of the lasers and positioning of the sampling gate were controlled by a programmable time-delay generator (Stanford Research Systems, DG535), which was in turn controlled by the Macintosh SE by way of a general purpose interface bus (GPIB). Background contributions to the signal from L_1 and L_2 alone were subtracted out following every 100 $L_1 + L_2$ pulses by firing the lasers individually. Background signal due to each reagent gas alone was also subtracted out by performing the experiment with one reagent gas at a time.

The main contribution to the background signal was from the direct photodissociation of the reagent DCl to form D and Cl. A background signal ranging over several masses in the region of mass 35 was observed when both reagents were flowing. The atomic Cl signal was clearly evident on top of this background. The contribution to the Cl signal from this background was subtracted by measuring the background signal with the probe laser tuned away from the REMPI wavelength for Cl. The atomic reagent (H) and products (D or Cl) were measured at the appropriate wavelengths as a function of time by changing the time delay, Δt, between lasers L_1 and L_2. Measurement of these signals as a function of Δt made possible determination of the diffusion lifetimes and the signal maxima.

Photolysis wavelengths were those of an excimer laser (Lumonics TE-861T-4, unstable resonator) operating at 193, 222, or 248 nm. Typical laser powers were in the range 0.2–15 mJ/pulse at a repetition rate of 50 Hz. The laser beam was focused to a spot size of approximately 2-mm diameter centered 3 mm below the nozzles.

The atomic species H, D, Cl, and Cl* were probed by using 2 + 1 resonantly enhanced multiphoton ionization (REMPI) at wavelengths in the range 235.33–243.13 nm. These wavelengths (243.134, 243.068, 235.336, and 237.808 nm) were obtained by doubling the output of a Lambda Physik dye laser operating in the range 470–487 nm (Coumarin 480 laser dye), using a β-barium borate doubling crystal (65°, 4 × 4 × 7 mm). The doubled output was separated from the fundamental beam by means of a CaF_2 Pellin-Broca prism. Pulse energies in the range 1.5–2.8 mJ/pulse at a repetition rate of 50 Hz were obtained for the doubled output. The probe laser beam was also focused to a spot size of approximately 2-mm diameter and was carefully overlapped with the photolysis laser beam.

In all cases the H, D, and Cl signals were normalized with respect to both the photolysis and probe laser powers. Laser power studies of the reagents have shown that the photolysis and probe lasers have respective power dependences of ~1 and ~2 for all of the atomic species.

The H and D signals were corrected for Doppler broadening, which is double the maximum Doppler shift of $\Delta\nu = \nu_0[v/c]$, where ν_0 is the probe frequency, v is the estimated velocity of the detected species, and c is the speed of light. Although a Doppler-broadened peak may show some structure due to anisotropy of motion following photodissociation,[20-23] at the short delay times involved, the peak was assumed to be still approximately rectangular.[23] This approximation accounted for the area under the H atom line (the salient quantity) to within approximately 20%. At 1-eV collision energy the H atom Doppler width was 9 times the laser bandwidth. The Cl signal was not corrected for Doppler broadening since $2\Delta\nu$ (~0.2 cm^{-1}) is smaller than the laser bandwidth (~0.425 cm^{-1}). For D, produced in the exchange reaction, Doppler broadening can be a significant correction (as in the case of reagent H); for example, at a center-of-mass collision energy of 1.20 eV, the departing D atom can have a velocity as high as 1.3×10^6 cm/s. (This is for the case that HCl is formed in the $v = 0$ state.) This leads to a peak Doppler-broadened to $2\Delta\nu = 2.97$ cm^{-1}, 7 times the laser bandwidth at a probe wavelength of 243.07 nm. The choice of width for the rectangular profile of D was based on sample trajectories; the error in representing the area under the D atom line was small in comparison with the experimental uncertainty in the exchange reaction cross sections.

The reagent gases H_2S (99.99%, Scott Specialty Gases), HBr (99.8% liquid phase, Matheson), HI (98.0% liquid phase, Matheson), and DCl (99% minimum D atom purity, Merck, Sharp and Dohme) were used without further purification.

Photolysis of H_2S gives nearly monoenergetic H atoms with 90%, 82%, and 95% of the HS photodissociation product formed in the $v = 0$ state at 193, 222, and 248 nm, respectively.[24,25] This produces "hot" H atoms with energies of 1.06, 1.62, and 2.44 eV at the photolysis wavelengths of 248, 222, and 193 nm. Photolysis of HBr and HI can lead to the formation of the halogen in either the ground ($^2P_{3/2}$) or excited ($^2P_{1/2}$) states. Photolysis of HBr at 248 nm leads very largely[26] to the formation of $Br(^2P_{3/2})$, resulting in energetic H atoms at 1.23 eV. The photolysis of HI has been variously estimated to give a ratio of $I(^2P_{3/2})/I^*(^2P_{1/2})$ of 0.43 ± 0.04[27] or 0.50 ± 0.03[28] at 248 nm and 0.55 ± 0.25[29]

(18) Collings, B. A.; Polanyi, J. C.; Smith, M. A.; Stolow, A.; Tarr, A. W. *Phys. Rev. Lett.* **1987**, *59*, 2551; **1989**, *63*, 2160.
(19) Sanzone, G. *Rev. Sci. Instrum.* **1970**, *41*, 741.
(20) Xu, Z.; Koplitz, B.; Buelow, S.; Baugh, D.; Wittig, C. *Chem. Phys. Lett.* **1986**, *127*, 534.
(21) Xu, Z.; Koplitz, B.; Wittig, C. *J. Chem. Phys.* **1987**, *87*, 1062.
(22) Xu, Z.; Koplitz, B.; Wittig, C. *J. Phys. Chem.* **1988**, *92*, 5518.
(23) Matsumi, Y.; Tonokura, K.; Kawasaki, M.; Ibuki, T. *J. Chem. Phys.* **1990**, *93*, 7981.
(24) Oldershaw, G. A.; Porter, D. A.; Smith, A. *J. Chem. Soc., Faraday Trans. 1* **1972**, *68*, 2218.
(25) Van Veen, G. N. A.; Mohamed, K. A.; Baller, T.; De Vries, A. E. *Chem. Phys.* **1983**, *74*, 261.
(26) Mulliken, R. S. *J. Chem. Phys.* **1940**, *8*, 382.
(27) Van Veen, G. N. A.; Mohamed, K. A.; Baller, T.; De Vries, A. E. *Chem. Phys.* **1983**, *80*, 113.
(28) Wight, C. A.; Leone, S. R. *J. Chem. Phys.* **1983**, *79*, 4823.
(29) Cadman, P.; Polanyi, J. C. *J. Phys. Chem.* **1968**, *72*, 3715.

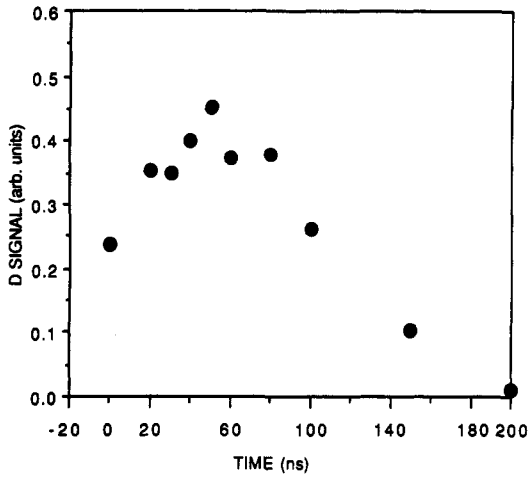

Figure 1. Exchange reaction product, D, as a function of time for a collision energy of 1.02 eV.

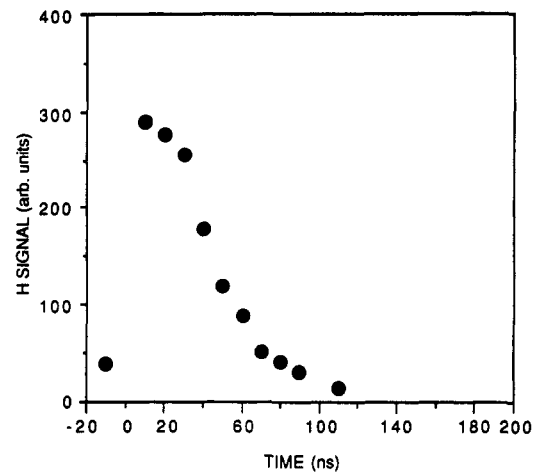

Figure 2. Reactant H atom signal (signal on the same scale as in Figure 1) as a function of time. The H atoms were produced by the photolysis of H_2S at 248 nm.

at 253.7 nm. In these experiments HI was photolyzed only at 248 nm. The resulting center-of-mass collision energies are 0.96 and 1.85 eV.

III. Experimental Reaction Cross Section

The rate of change of concentration of the D or Cl atomic products in the volume under observation (the "reaction region") can be expressed as the sum of the rate of formation and the rate of diffusion of the product out of the reaction region. The rate of change of $[D(t)]$, the product of exchange reaction, takes the following form

$$d[D(t)]/dt = \sigma_{ex} v [H(t)][DCl] - [D(t)]/\tau$$

where the first term on the right represents the rate of reaction and the second term the diffusion rate of D out of the interaction region. In this expression σ_{ex} is the exchange reaction cross section, v is the relative collision velocity of the H and DCl, and τ is the diffusion lifetime of the product D. The concentration of some species X at a given time, $[X(t)]$, is related to the MPI signal, $S_X(t)$, by a time-independent proportionality factor c_X which depends on the detection efficiency and the abundance of X. We denote the times of the maximum signals for the H, D, and Cl curves as t_H, t_D, and t_{Cl}, respectively.

At t_D, the maximum in the $D(t)$ curve, we set $d[D(t)]/dt$ equal to zero and rearrange to obtain

$$\sigma_{ex} = \frac{1}{v\tau[DCl]} \frac{[D(t_D)]}{[H(t_D)]} \tag{1}$$

where we have assumed $c_H = c_D$ and hence $S_H/S_D = [H]/[D]$.

At the center-of-mass collision energy, E_{coll}, of 1.02 eV the velocity, v, is 1.4×10^6 cm/s, $\tau \approx 40 \pm 5$ ns, and $[DCl] = (7 \pm 2) \times 10^{14}$ molecules/cm^3 (20 mTorr; see Appendix A). The ratio $[D(t_D)]/[H(t_D)]$ was measured as $(2.5 \pm 0.6) \times 10^{-3}$ at a time $t_D = 50$ ns (see Figure 1). This yielded an absolute cross section for exchange, $\sigma_{ex} \approx 0.6 \pm 0.3$ Å^2.

In general, due to temporal drift of the photolysis laser, it was found to be experimentally more accurate to measure the reagent $[H(t)]$ at its maximum (t_H). This was done to avoid the measurement of $[H(t)]$ in a region where the combination of a rapidly changing $d[H(t)]/dt$ or low signal-to-noise ratio (Figure 2) and a timing error could decrease the precision of measurement. The exchange reaction cross sections at various collisions, E', were then referenced to the measured exchange cross section at $E = 1.02$ eV. The ratio of σ_{ex} at energies $E = 1.02$ eV and other energies $E = E'$ gives the expression

$$\frac{\sigma_{ex}(E')}{\sigma_{ex}(1.02)} = \frac{v(1.02)\tau_D(1.02)[DCl]}{v(E')\tau_D(E')[DCl]} \left(\frac{[D(t_D)]}{[H(t_D)]}\right)_{E'} \left(\frac{[H(t_D)]}{[D(t_D)]}\right)_{1.02} \tag{2}$$

where, due to the fact that we are dealing with ratios, $S_X(t)$ or $[X(t)]$ can be used interchangeably. The experimental $[H(t)]$ curves were all similar in form (though the absolute concentrations were dependent upon the photolysis laser intensity and the photodissociation cross section of the H atom precursor). This implies that $[H(t)]_{1.02} = \gamma[H(t)]_{E'}$ where γ is a proportionality constant; consequently, the term involving concentration ratios can be replaced by

$$\left(\frac{[D(t_D)]}{[H(t_H)]}\right)_{E'} \left(\frac{[H(t_H)]}{[D(t_D)]}\right)_{1.02} \tag{3}$$

Substituting (3) into (2) then gives for $\sigma_{ex}(E')$

$$\sigma_{ex}(E') = \sigma_{ex}(1.02) \frac{v(1.02)}{v(E')} \left(\frac{[D(t_D)]}{[H(t_H)]}\right)_{E'} \left(\frac{[H(t_H)]}{[D(t_D)]}\right)_{1.02} \tag{4}$$

Measurement of the abstraction reaction cross section was made by referencing it to the known exchange cross section (eq 4) at the same collision energy

$$\sigma_{ab}(E') = \sigma_{ex}(E') \left(\frac{S_{Cl}(t_{Cl})}{S_D(t_D)}\right)_{E'} \Phi \tag{5}$$

The signals S_{Cl} and S_D are explicitly shown since $c_{Cl} \neq c_D$. The value $\sigma_{ex}(E')$ was that calculated above, using eq 4. The correction factor Φ was employed to compensate for the difference in diffusion rates, detection efficiency of Cl relative to D (see below), and the natural isotopic abundance of ^{35}Cl and ^{37}Cl (a factor of 1.320):

$$\Phi = \frac{[D(t_D)]_d}{[Cl(t_{Cl})]_d} \frac{1}{\epsilon}(1.320) \tag{6}$$

The first term in eq 6 corrects for the difference in rates of diffusion of D and Cl from the reaction zone. The concentration ratio $[D(t_D)]_d/[Cl(t_{Cl})]_d$ was taken from a model of the concentration profiles based on equal rates of formation of the two species, with rates of diffusion from the reaction zone obtained from fits to the experimental data at long times. It was obtained from the following relations:

$$[D(t)]_d = \exp(-t/\tau_D) \int_0^t \exp(t'/\tau_D) \sigma_{ex} v [H(t')][DCl]\, dt' \tag{7}$$

$$[Cl(t)]_d = \exp(-t/\tau_{Cl}) \int_0^t \exp(t'/\tau_{Cl}) \sigma_{ab} v [H(t')][DCl]\, dt' \tag{8}$$

The derivation of eqs 7 and 8 is given in Appendix B. The parameters τ_D and τ_{Cl} in eqs 7 and 8 are the diffusion lifetimes. The reagent $[H(t)]$ curve was modeled by convoluting the photolysis laser pulse shape with the diffusion of the H atom, using

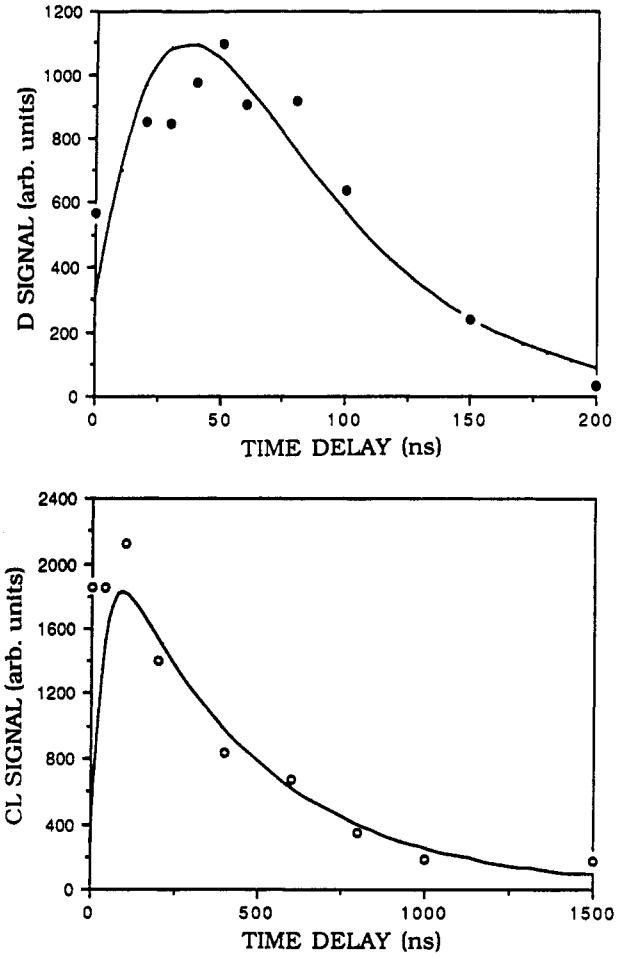

Figure 3. Reaction product concentrations as a function of time: D above, Cl below. The curves were calculated from eqs 7 and 8 and normalized for best fit at long times. The points are experimental.

τ_H (see Appendix B). The $[D(t)]_d$ and $[Cl(t)]_d$ curves were convoluted with the pulse shape of the probe laser (fwhm $\approx$ 25 ns) resulting in typical concentration profiles as shown in Figure 3, with corresponding experimental points shown for comparison.

The detection efficiency ϵ of $Cl(^2P_{3/2})$ relative to D was determined by measuring the relative intensity of the photodissociation products of DCl at 193 nm. The signals were measured at their maxima and were also corrected for differing rates of diffusion out of the interaction region. A detection efficiency for $Cl(^2P_{3/2})$ relative to D of 0.4 ± 0.1 was found after corrections for the formation of $Cl(^2P_{3/2})$ and $Cl^*(^2P_{1/2})$ and the natural isotopic abundance of ^{35}Cl to ^{37}Cl.

The photodissociation of DCl leads to the formation of both $Cl(^2P_{3/2})$ and $Cl^*(^2P_{1/2})$. Tiemann et al.[30] have photodissociated HCl at 193 nm and found 67% $Cl(^2P_{3/2})$ and 33% $Cl^*(^2P_{1/2})$. In the present study the measurement of $Cl(^2P_{3/2})$ and $Cl^*(^2P_{1/2})$ in the photodissociation of HCl at 193 nm by 2 + 1 REMPI through the $^2D_{3/2}$ state showed that the signal from $Cl(^2P_{3/2})$ was 5.3 ± 0.5 times more intense than that from $Cl^*(^2P_{1/2})$.

Using the $Cl(^2P_{3/2})/Cl^*(^2P_{1/2})$ ratio from the photodissociation of HCl at 193 nm, we obtained a value of 2.7 ± 0.3 for the detection efficiency of $Cl(^2P_{3/2})$ relative to $Cl^*(^2P_{1/2})$. The measurement of $Cl(^2P_{3/2})$ and $Cl^*(^2P_{1/2})$ in the photodissociation of DCl at 193 nm, once again through the $^2D_{3/2}$ state, showed that the signal from $Cl(^2P_{3/2})$ was 11.7 ± 1.4 times that for $Cl^*(^2P_{1/2})$ signal. This corresponds to the formation of 81 ± 3% and 19 ± 3% atomic chlorine in the $^2P_{3/2}$ and $^2P_{1/2}$ states, respectively, during the photodissociation of DCl at 193 nm, when corrected for the measured detection efficiency of 2.7 ± 0.3 for $Cl(^2P_{3/2})/Cl^*(^2P_{1/2})$.

(30) Tiemann, E.; Kanamori, H.; Hirota, E. *J. Chem. Phys.* **1988**, *88*, 2457.

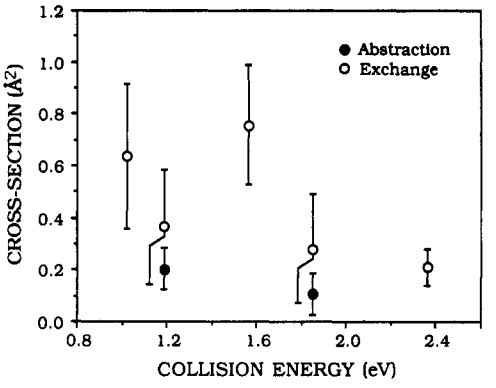

Figure 4. Experimental reaction cross sections for the abstraction (solid circles) and exchange (open circles) channels as a function of collision energy.

TABLE I: Center-of-Mass Collision Energies (H + DCl) for Laser Photolysis of the Stated Precursor at the Indicated Wavelengths

precursor	wavelength, nm	energies, eV
H_2S	248	1.02[b]
H_2S	222	1.56[b]
H_2S	193	2.36[b]
HBr	248	1.19 (0.75)[a]
HI	248	0.96 (50%), 1.85 (50%)[c]

[a] The photolysis of HBr at 248 nm leads predominantly to the formation of bromine in its ground electronic state.[26] [b] References 24 and 25. [c] References 27–29.

The chlorine products were probed at a time of 40 ns, and thus diffusion of $Cl(^2P_{3/2})$ and $Cl^*(^2P_{1/2})$ out of the reaction volume, and also relaxation of $Cl^*(^2P_{1/2})$ through quenching, were negligible.

The measured power dependence for the probe laser was ~2, rather than the anticipated value of 3. This suggests that saturation of the final REMPI step was occurring, i.e., all $Cl(^2D_{3/2}) \rightarrow Cl^+$; thus the two-photon step became the limiting one. A possible complication could arise from the presence of a substantial ac Stark shift. However, a frequency scan showed that at laser powers of $\sim 10^6$ W/cm^2 the line shift due to the second-order ac Stark effect was negligible in comparison to the laser bandwidth of 0.425 cm^{-1}. In the absence of a significant Stark shift the observed power dependence indicates saturation of the ionization step. The detection efficiency is equal to the ratio of the two-photon transition probabilities for the transitions $^2D_{3/2} \leftarrow {}^2P_{3/2}$ and $^2D_{3/2} \leftarrow {}^2P_{1/2}$.

IV. Experimental Results

The reaction cross sections for the exchange and abstraction channels as a function of the center-of-mass collision energy over the range 1.0–2.4 eV are shown in Figure 4. Each cross section is the average of three or more measurements. Table I summarizes the precursors and wavelengths used in these experiments.

The results for the abstraction channel, at the two collision energies 1.19 and 1.85 eV, are for the formation of chlorine in the ground state ($^2P_{3/2}$). In the case of the HI precursor photolyzed at 248 nm, the abstraction product signal was a combination of the product at collision energies 0.96 and 1.85 eV resulting from the 50:50 formation of I and I*.[27-29] The cross section shown at 1.85 eV was corrected for the low-energy contribution assuming $\sigma_{ab}(0.96) \approx \sigma_{ab}(1.2)$. The formation of chlorine in the excited state (reaction 1*) was not observed, leading to an upper limit of 0.02 Å^2 for the reaction cross section.

The abstraction cross section, σ_{ab}, remains nearly constant at an average value of 0.16 ± 0.06 Å^2. This value is in good agreement with the value for σ_{ab} obtained from the best available potential energy surface for this reaction (see below). It is, however, substantially smaller than the reaction cross section for H + HCl abstraction at 1.6-eV collision energy reported by Aker et al.[14] of 2.0 ± 1.0 Å^2. In that experiment they monitored the formation of the diatomic product H_2 in the reaction H + HCl

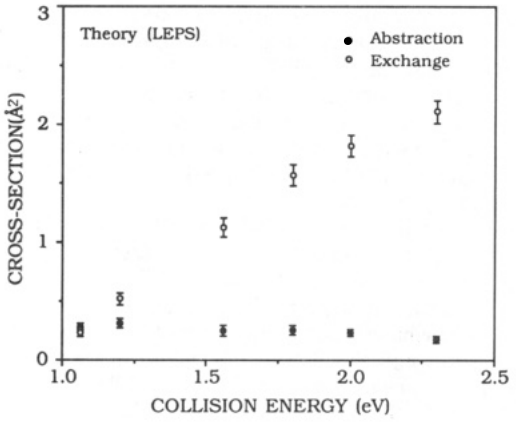

Figure 5. Reaction cross sections for the abstraction (solid circles) and exchange (open circles) as calculated by a quasi-classical trajectory method[31] using the GQQ PES of Schwenke et al.[12]

using CARS spectroscopy; their cross section is the sum of the cross sections for abstraction leading to the formation of both $Cl(^2P_{3/2})$ and $Cl^*(^2P_{1/2})$.

Observation of the abstraction reaction at the collision energies 1.02, 1.56, and 2.36 eV was not possible owing to the difficulty of measuring the atomic chlorine product in the presence of a large ion signal at mass 34 (H_2S^+ formed by the probe laser) which saturated the detector, obscuring signals from masses 35 and 37.

Measurement of the reaction cross section for the exchange channel showed a moderate decrease as the collision energy was increased from 1.02 to 2.36 eV (Figure 4). The exchange cross section was an average of ~3 times that for abstraction. The reaction cross section for exchange at 1.85 eV (HI at 248 nm) was calculated assuming $\sigma_{ab}(0.96) \approx \sigma_{ab}(1.02)$.

V. Quasi-Classical Trajectory Calculations

A total of 4000 quasi-classical trajectories (QCT) were computed at each collision energy to determine the reaction cross sections, using the algorithm of Karplus et al.[31] The potential energy surface (PES) used in our calculation was the recently developed "global" GQQ surface.[12] This PES has been used by Aker et al.[32] to model and compare the rovibrational distribution of the H_2 product in the reaction H + HCl to their experimental results at a collision energy of 1.6 eV.[14]

The GQQ PES was formed by adding a barrier term for exchange to the LEPS potential energy surface termed GSW, from the work of Stern, Persky, and Klein.[6] The parameter values of this additional term, which was a function of the three internuclear distances and the H–Cl–H angle, were determined by these workers[12] by fitting to several high-quality ab initio points in the collinear and near-collinear saddle point regions. The collinear exchange barrier on the GQQ surface was 18.1 kcal/mol while the collinear abstraction barrier was 4.6 kcal/mol.

As shown in Figure 5, the QCT reaction cross section for the abstraction channel decreases slightly, from 0.31 to 0.18 Å², as the collision energy is increased from 1.0 to 2.4 eV. The fact that there is no striking change in cross section as the collision energy is increased is consistent with the experimental findings. The calculated reaction cross sections are in good agreement with the experimental cross sections at all energies.

The most obvious difference between experiment and the theory is to be found in the marked increase in exchange reaction cross section with collision energy from theory (Figure 5), as compared to the moderate decline found experimentally (Figure 4). At E_{coll} = 1.0 eV the exchange cross section is somewhat lower than that observed experimentally while at E_{coll} = 2.3 eV the exchange cross section is an order of magnitude too high.

Further examination of the features of the PES was carried out by plotting the geometries of closest approach for reactive trajectories on rigid-molecule plots. In such a plot the D–Cl separation is held constant and potential energy contours are given for H atom approach. The criterion for the closest approach geometry is defined as the configuration giving the minimum sum of H–D and H–Cl distances in the course of a trajectory. The internuclear separations as a function of time for a sample trajectory leading to abstraction are shown in Figure 6; the point of closest approach is indicated by the position of the broken line.

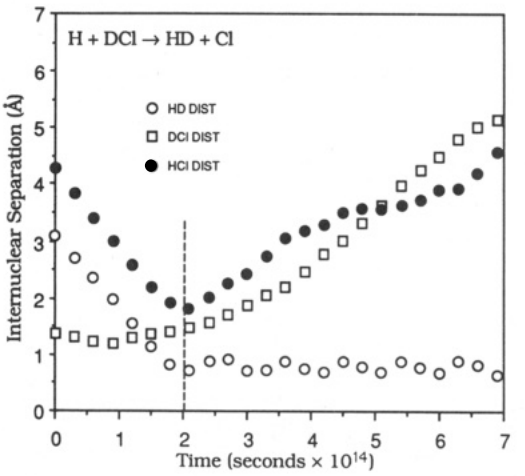

Figure 6. Internuclear separations as a function of time for a trajectory leading to abstraction at the collision energy of 1.06 eV. The broken line indicates the point at which the closest approach criterion is met.

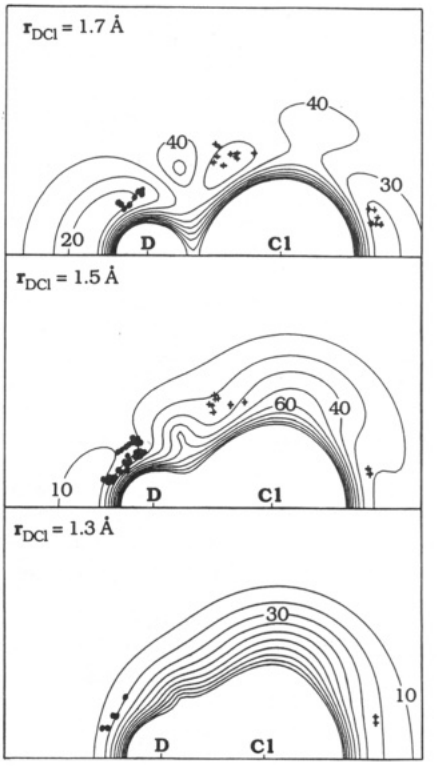

Figure 7. Rigid-molecule plots showing the geometries of closest approach in H + DCl collisions at 1.06 eV. Each plot represents a range of ±0.1 Å about the D–Cl separation indicated. Geometries leading to abstraction are indicated by the closed circles while those leading to exchange are indicated by crosses. Contours are labeled in kcal/mol, relative to H + DCl; the contour interval is 10 kcal/mol.

Figure 7 shows closest approach geometries on the rigid-molecule plots at 1.06-eV collision energy, for three different D–Cl internuclear separations. Each rigid-molecule plot covers a small range of D–Cl separations (see caption). Not all D–Cl separations involved in the closest approach geometries are pictured; the range of D–Cl separations extended to D–Cl ≈ 2.1 Å. The total number of trajectories used to obtain the results shown in Figure 7 was 4800, of which 45 resulted in abstraction and 61 in exchange. The

(31) Karplus, M.; Porter, R. N.; Sharma, R. D. *J. Chem. Phys.* **1965**, *43*, 3259.
(32) Aker, P. M.; Valentini, J. J. *Isr. J. Chem.* **1990**, *30*, 157.

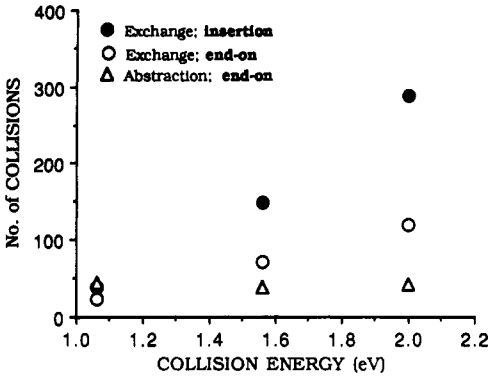

Figure 8. Frequency of trajectories leading to abstraction (△), exchange by insertion (●), and exchange by an end-on approach (○) as a function of collision energy. The total number of trajectories is 4800 at each collision energy.

majority of closest approach geometries for E_{coll} = 1.06 eV occurred within a D–Cl separation of 1.3–2.1 Å whereas at E_{coll} = 2.0 eV (not shown) this range extended from 1.3 to 2.5 Å.

Examination of Figure 7 reveals that for trajectories leading to *abstraction* at 1.06-eV collision energy (well in excess of the collinear abstraction barrier of 0.2 eV) the preferred geometry is noncollinear with a H–D–Cl angle lying in the range 95–155°. The majority of the closest approach geometries leading to abstraction occur at relatively short D–Cl separations, 1.2–1.7 Å.

Examination of the closest approach geometries which lead to *exchange* (also Figure 7) shows two distinct geometries: the H atom can approach the D–Cl either from the side, inserting itself between the D and Cl, or end-on from the Cl of D–Cl in a nearly collinear approach. The end-on geometries occur over a D–Cl separation of 1.2–2.0 Å and a range of H–Cl–D angles from 150° to 165°. By contrast, the range of H–Cl–D angles for the insertion mechanism is 55–80°. The majority of the insertions occur with the D–Cl separation between 1.4 and 2.0 Å. The prevalence of highly bent configurations indicates the importance of the PES in this nonlinear region.

Insertion appears to be the pathway that opens up at high collision energy, giving the exchange cross section its strong collision energy dependence; see upper curve in Figure 8. Lateral insertion in hot-atom reactions involving the light plus light–heavy mass combination was also noted in early studies.[33] The frequency of occurrence of the insertion and end-on exchange geometries as a function of collision energy in the present work is shown in Figure 8. The probability of abstraction stays constant at a low value.

The constancy of the experimental exchange cross section with increasing collision energy in contrast to the rapid increase predicted by the theory suggests that the potential energy the H atom encounters as it approaches the DCl on the GQQ PES is not repulsive enough in the side-approach region; i.e., insertion should still be energetically prohibited at 1–2-eV collision energies.

VI. Conclusion

The cross sections for the abstraction and exchange reactions H + DCl → HD + Cl (I) and → HCl + D (II) have been measured as a function of collision energy over the range 1.0–2.4 eV. The atomic product was observed by means of REMPI and time-of-flight mass spectrometry.

The results for abstraction showed no significant change in reaction cross section with respect to collision energy. For exchange they showed a marginal decrease in cross section with increasing collision energy. The cross section for abstraction was approximately one-half to one-third that for exchange throughout this range of collision energies. The abstraction channel leading to the formation of excited-state chlorine did not contribute, over the energy range studied.

The experimentally measured reaction cross sections were compared with those obtained from quasi-classical trajectory calculations using the GQQ PES. The calculated abstraction cross sections were in good agreement with experimental results. The calculated exchange cross sections, however, were not, and the resulting differences pointed to a poorly understood region of the PES. Examination of the closest approach geometries for sample trajectories suggested that the deficiency in the GQQ PES might derive from an incorrect rendering of the repulsive interaction which, for high collision energies, permits facile lateral insertion of H into the extending DCl bond.

The GQQ surface was fitted accurately by Schwenke et al.[12] to within a few hundreths of an electronvolt of the ab initio data. The ab initio points that determined the parameters of the GQQ potential were however restricted to the saddle-point regions of the collinear PES, with very limited data for the saddle points of noncollinear geometries. It would seem that a wider range of ab initio points is needed, as well as inclusion of nonadiabatic transitions that may decrease the reaction probability for approach from the Cl end of DCl.

Acknowledgment. We thank P. M. Aker, E. Hirota, and J. J. Sloan for helpful discussions. This work was made possible through the generous support of the Natural Sciences and Engineering Research Council of Canada (NSERC), the Venture Research Unit (BP Canadian Holdings Limited), and the Ontario Laser and Lightwave Research Centre. V.B. thanks NSERC for the award of a Postdoctoral Fellowship.

Appendix A. Calculation of DCl Density in the Reaction Region

The density of DCl in the reaction region was calculated by using the equations for expansion of a diatomic gas from a free jet.[34] The density, n, can be expressed in terms of the density at the nozzle outlet, n_0, as

$$n = n_0[1 + 0.5(\gamma - 1)M_{eff}^2]^{-1/(\gamma-1)} \quad \text{(A1)}$$

where γ is the heat capacity ratio C_p/C_v for DCl and M_{eff} is the effective Mach number, determined via the formula[34]

$$M_{eff} = 3.65(x/D - 0.4)^{0.4} - 0.82(x/D - 0.4)^{-0.4} \quad \text{(A2)}$$

where x is the distance from the nozzle to the reaction region and D is the nozzle diameter.

For $n_0 = 4.8 \times 10^{18}$ molecules/cm^3 (140 Torr), $\gamma = 1.40$, $x = 3$ mm, and $D = 0.12$ mm, the value of M_{eff} is 13, and n is calculated to be $(7 \pm 2) \times 10^{14}$ molecules/cm^3 (20 mTorr).

The pressure at the nozzle outlet, P_0, which is proportional to n_0, was calculated by using Poiseuille's formula

$$P_0 = (-dV/dt)8\eta L/\pi a^4 + P_1 \quad \text{(A3)}$$

where dV/dt is the flow rate, η is the viscosity of the DCl, L is the nozzle length, a is the internal radius of the nozzle, and P_1 is the nozzle backing pressure. Substituting $dV/dt = 5.5 \times 10^{-8}$ m^3 s^{-1}, $\eta = 1.43 \times 10^{-5}$ kg m^{-1} s^{-1}, $L = 5.08 \times 10^{-2}$ m, $a = 6 \times 10^{-5}$ m, and $P_1 = 2.67 \times 10^4$ kg m^{-1} s^{-1} (200 Torr) gave a value of 1.87×10^4 kg m^{-1} s^{-1} (140 Torr) for P_0.

Appendix B. Modeling the Rate of Product Formation

The rate of change of photodissociation product H takes the form

$$\frac{d[H(t)]}{dt} = f(t) - \frac{[H(t)]}{\tau_H} \quad \text{(B1)}$$

where τ_H is the diffusion lifetime of H and $f(t)$ the intensity of the photolyzing laser pulse as a function of time. Equation B1 is a first-order linear differential equation

$$\dot{y} + y/\tau_H = f(t) \quad \text{(B2)}$$

(33) Kuntz, P. J.; Nemeth, E. M.; Polanyi, J. C.; Wong, W. H. *J. Chem. Phys.* **1970**, *52*, 4654.

(34) Lubman, D. M.; Rettner, C. T.; Zare, R. N. *J. Phys. Chem.* **1982**, *86*, 1129.

Multiplying both sides of (B2) by $\exp(t/\tau_H)$ we obtain

$$\dot{y}\exp(t/\tau_H) + (y/\tau_H)\exp(t/\tau_H) = f(t)\exp(t/\tau_H)$$

We can use the identity $d(xy)/dt = \dot{x}y + x\dot{y}$ which gives

$$d(y\exp(t/\tau_H))/dt = f(t)\exp(t/\tau_H)$$

which can then be integrated to determine the concentration $y = [H(t)]$ at a given time $t = t'$:

$$y\exp(t/\tau_H)|_{t=t'} = \int_0^{t'} f(t)\exp(t/\tau_H)\,dt + C$$

$$y(t') = \exp(-t'/\tau_H)\int_0^{t'} f(t)\exp(t/\tau_H)\,dt + C \quad (B3)$$

At $t = 0$ the value of the integral is zero, leaving $y(t') = C$. The boundary condition $y(t') = 0$ exists which implies that $C = 0$.

The rate of product formation may be written

$$\frac{d[H(t)]}{dt} = k[H(t)][DCl] - \frac{[H(t)]}{\tau_H} \quad (B4)$$

Assuming [DCl] remains constant over time we have $k[DCl] = k'$, and (B4) may then be written in a form analogous to (B2):

$$\dot{z} + z/\tau_H = k'y(t)$$

and solved to give at the time of detection, $t = t_d$:

$$z(t_d) = \exp(-t_d/\tau_P)\int_0^{t_d} k'y(t')\exp(t'/\tau_P)\,dt'$$

Substituting in (B3) we obtain an expression for the product concentration at time t_d, $[P(t_d)] = z(t_d)$:

$$z(t_d) = \exp\left(\frac{-t_d}{\tau_P}\right)\int_0^{t_d} k'\exp\left(\frac{-t'}{\tau_H}\right)\times\left[\int_0^{t'} f(t)\exp\left(\frac{t}{\tau_H}\right)dt\right]\exp\left(\frac{t'}{\tau_P}\right)dt' \quad (B5)$$

The integral in (B3) can be approximated by

$$\sum_{i=0}^{m} f(t_i)\exp(t_i/\tau_H)h$$

which when substituted into eq B3 gives

$$[H(t_m)] = \exp(-t_m/\tau_H)\sum_{i=0}^{m}\{f(t_i)\exp(t_i/\tau_H)h\} \quad (B6)$$

where h is the width of the interval used in the summation. In this study the summation was performed using 0.5-ns increments.

Similarly, the integral in (B5) can be approximated by

$$\sum_{j=0}^{n} k'\left[\exp\left(\frac{-t_m}{\tau_H}\right)\sum_{i=0}^{m}\left\{f(t_i)\exp\left(\frac{t_i}{\tau_H}\right)h\right\}\right]\exp\left(\frac{t_j'}{\tau_p}\right)h$$

to give

$$[P(t_n)] = \exp\left(\frac{t_n}{\tau_p}\right)\times\sum_{j=0}^{n} k'\left[\exp\left(\frac{-t_m}{\tau_H}\right)\sum_{i=0}^{m}\left\{f(t_i)\exp\left(\frac{t_i}{\tau_H}\right)h\right\}\right]\exp\left(\frac{t_j'}{\tau_p}\right)h \quad (B7)$$

where $[P(t_n)]$ can be either $[D(t)]_d$ or $[Cl(t)]_d$ and τ_P is either τ_D or τ_{Cl}.

Matrix Isolation and Mass Spectrometric Studies of the Vaporization of Alkali Metal Oxoselenium Salts: Characterization of Molecular M_2SeO_4, M_2SeO_3, and $MSeO_2$

Alan K. Brisdon, Robin A. Gomme, and J. Steven Ogden*

Department of Chemistry, The University, Southampton SO9 5NH, UK *(Received: October 5, 1990)*

Solid samples of alkali metal selenates (M_2SeO_4) and selenites (M_2SeO_3) have been heated in vacuo, and the vaporization products studied by using a combination of mass spectrometric and matrix isolation IR techniques. Although some decomposition was observed, evidence was obtained for the existence of the ternary molecular salts M_2SeO_4 and M_2SeO_3 (M = Na, K, Rb, Cs) and also for the novel Se(III) species $MSeO_2$. The molecular symmetries are identified as D_{2d}, C_s, and C_{2v}, respectively, on the basis of vibrational selection rules, and the various O–Se–O bond angles in these species are estimated from selenium isotope shifts and relative band intensities.

Introduction

Until relatively recently, our knowledge of alkali metal sulfates and selenates has largely been confined to the condensed phases, and the chemistry of these salts has been extensively documented. However within the past 20 years, it has been found that anhydrous sulfates can be sublimed in vacuo to yield molecular M_2SO_4 species. These ternary molecules were originally identified by mass spectrometry,[1] and subsequent electron diffraction studies indicated that their structures are based on bisbidentate coordination, leading to D_{2d} symmetry.[2] This model was later supported by matrix isolation studies.[3,4]

Corresponding experiments on the vaporization of alkali metal sulfites do not appear to have been carried out, but it has been shown that under matrix conditions, the cocondensation of Tl_2O and SO_2 yields molecular Tl_2SO_3.[5] The third known member of this series of molecular sulfur oxo anion salts is provided by the electron-transfer reaction between an alkali metal and SO_2 in low temperature matrices. This reaction leads to ion pair molecules of general stoichiometry MSO_2.[6]

In contrast to these studies on sulfur oxo anion salt molecules, nothing is known about the existence of selenium analogues. Alkali metal selenates and selenites reportedly undergo complex thermal decompositions on heating,[7,8] leading to a variety of solid products,

(1) See, e.g.: Buchler, A.; Stauffer, J.; Klemperer, W. *J. Chem. Phys.* **1967**, *46*, 605.
(2) Spiridonov, V. P.; Lutoshkin, B. I. *Vest. Mosk. Univ. Ser. Khim.* **1970**, *No. 6*, 509.
(3) Atkins, R. M.; Gingerich, K. A. *Chem. Phys. Lett.* **1978**, *53*, 347.
(4) Belyaeva, A. A.; Dvorkin, M. I.; Shcherba, L. D. *Opt. Spectrosc.* **1971**, *31*, 309.
(5) David, S. J.; Ault, B. S. *Inorg. Chem.* **1984**, *23*, 1211.
(6) Milligan, D. E.; Jacox, M. E. *J. Chem. Phys.* **1971**, *55*, 1003.
(7) Giolito, I.; Ionashiro, M. *Thermochim. Acta* **1980**, *38*, 341.
(8) Selivanova, N. M.; Schneider, V. A.; Streltsov, I. S. *Russ. J. Inorg. Chem.* **1959**, *4*, 667. Selivanova, N. M.; Schneider, V. A.; Streltsov, I. S. *Russ. J. Inorg. Chem.* **1960**, *5*, 1101.

0022-3654/91/2095-2927$02.50/0